PERGAMON

International Journal of Heat and Mass Transfer 42 (1999) 889–903

International Journal of HEAT and MASS TRANSFER

Determination of operation envelopes for closed, two-phase thermosyphons

Mohamed S. El-Genk*, Hamed H. Saber

Institute for Space and Nuclear Power Studies/Department of Chemical and Nuclear Engineering, University of New Mexico, Albuquerque, NM 87131, U.S.A.

Received 24 July 1997; in final form 15 June 1998

Abstract

A concern in the design and operation of closed, two-phase therosyphons (CTPTs) is determining the initial filling ratio of the working fluid, as a function of CTPT dimensions, type and vapor temperature of working fluid and power throughput, to maximize performance, while avoiding potential dryout in the evaporator section. A one-dimensional, steady-state model is developed for determining the operation envelopes of CTPTs, in terms of the above parameters. The CTPT operation envelope is basically an enclosure with three boundaries. The lower boundary corresponds to when the liquid film thickness in the evaporator reaches a critical value—beyond it the liquid film could dry out—while the upper boundary corresponds to when the expanding liquid pool, due to boiling, fills the entire evaporator. The third and closing boundary corresponds to the counter-current flooding limit (CCFL) at the exit of evaporator. The correlation developed to calculate the expanded liquid pool height in the evaporator agrees with experimental data of acetone, ethanol and water to within $\pm 8\%$. Also, the calculated upper and lower boundaries of the operation envelope for an ammonia CTPT are in excellent agreement with experimental data [1]. Calculations showed that increasing the CTPT diameter, evaporator length, or vapor temperature expands the operation envelope, while increasing either the condenser or the adiabatic section length only slightly changes the envelope's upper and lower boundaries.

Nomenclature

A_{ei} evaporator inner surface area [m^2]
Bo Bond number based on d_i, $d_i(\sigma/(\Delta\rho g))^{-0.5}$
Bo_δ Bond number based on δ, $\delta(\sigma/(\Delta\rho g))^{-0.5}$
C_p specific heat capacity [J kg^{-1} K^{-1}]
C_o distribution parameter, equation (26)
d diameter [m]
D_h dimensionless hydraulic diameter $(d_i/\sqrt{\sigma/(g(\rho_l-\rho_g))})$
f friction coefficient, equation (13)
F^* dimensionless vapor velocity, $\bar{V}_g/ < V_{gj} >$
g gravitational acceleration [m s^{-2}]
Gr_{TP} two-phase Grashof number $(gd_i^3\rho_l\Delta\rho/\mu_l^2)$
h heat transfer coefficient [W m^{-2} K]
H_p expanded liquid pool height (L_p/L_e)
h_{fg} latent heat of vaporization [J kg^{-1}]
J_g vapor superficial velocity [m s^{-1}]
L length or height [m]
l_l liquid film thickness scale $(\mu_l^2/g\rho_l(\rho_l-\rho_g))^{1/3}$ [m]
l_m bubble length scale $(\sigma/g(\rho_l-\rho_g))^{0.5}$ [m]
k thermal conductivity [W m^{-1} K^{-1}]
m_{lp} working fluid inventory in pool [kg]
$N_{\mu f}$ viscosity number, $\mu_l/(\sigma\rho_l\sqrt{\sigma/(g(\rho_l-\rho_g))})^{0.5}$, equation (28)
P pressure [Pa]
Pr Prandtl number $(\mu C_p/k)$
Q power throughput [W]
R radius [m]
Ra Rayleigh number $(\beta g d_i^4 q_e/(k_l\alpha_l v_l))$
Re local film Reynolds number $(4\Gamma_f/\mu_l = 4q_e(L_e-x)/\mu_l h_{fg})$
Re_{ext} film Reynolds number at evaporator exit $(4Q/(\pi d_i h_{fg}\mu_l))$
T temperature [K]
$\bar{T}$ average temperature [k]

* Corresponding author. Tel: 001 505 277 5442; Fax: 001 505 277 2814; E-mail: mgenk@unm.edu

0017–9310/98/$—see front matter
PII: S0017–9310(98)00212–9

u flow velocity [m s^{-1}]
U conductance, equation (30) [W m^{-2} K], dimensionless flow velocity ($u/(\delta^2\Delta\rho g/(2\mu_l))$)
V_{gj} vapor drift velocity, $V_{gj}^{+}(\sigma g(\rho_l-\rho_g)/\rho_l^2)^{0.25}$ [m s^{-1}]
$\bar{V}_g$ mean vapor velocity at evaporator exit, $4q_eL_e/(\rho_g d_i h_{fg})$ [m s^{-1}]
V_{gj}^{+} dimensionless vapor drift velocity, equation (28)
x axial coordinate [m]
X dimensionless axial coordinate [x/L_e]
y lateral coordinate [m]
Y dimensionless lateral coordinate (y/δ).

Greek symbols
α void fraction, thermal diffusivity [m^2 s^{-1}]
β Thermal expansion coefficient [K^{-1}]
Γ mass flow rate per unit perimeter [kg m^{-1} s^{-1}]
δ liquid film thickness [m]
Δ dimensionless film thickness (δ/R_i)
ΔT_e evaporator wall superheat ($\bar{T}_{ei}-T_v$) [K]
ξ initial filling ratio of working fluid
μ dynamic viscosity [N s m^{-2}]
ν kinematics viscosity [m^2 s^{-1}]
ρ density [kg m^{-3}]
$\Delta\rho$ $(\rho_l-\rho_g)$ [kg m^{-3}]
σ surface tension [N m^{-1}]
τ shear stress [N m^{-2}]
τ^* dimensionless shear stress ($\tau/(\Delta\rho g d_i(1-\Delta))$)
Ψ pool mixing coefficient, equation (35).

Subscripts
a adiabatic section, adiabatic
c condenser section
cr critical
d dynamic
e evaporator section
f liquid film
i inner surface, L–V interface, initial
Ku Kutatelatze
l liquid
m mean, average
NB nucleate boiling
NC natural convection
p pool
v, g vapor
x local.

1. Introduction

The simple design and operation principle and the high heat transport capabilities of CTPTs are the primary reasons for their wide use in many industrial and energy applications. A design and operation concern, however, is determining the initial filling ratio of the working fluid, as a function of CTPT dimensions, type and vapor temperature of the working fluid, and the power throughput, to maximize the CTPT performance, while avoiding a potential dryout of the liquid film in the evaporator section (Fig. 1a). A local film dryout in the evaporator could occur when the rate of liquid return from the condenser decreases beyond that needed to maintain a continuous liquid film along the evaporator wall, above the liquid pool region (Fig. 1b). A reduction in the rate of liquid return to the evaporator could occur, either as a result of a low initial filling ratio of the working fluid (Fig. 1c) or reaching the counter current flooding limit (CCFL) at exit of the evaporator [2–6] (Fig. 1d). As shown in Fig. 1c, a liquid film dryout could occur in the evaporator, at a power throughput well below that at CCFL, when the liquid return from the condenser is insufficient to replenish the liquid pool in the evaporator. As a result, the recessed liquid pool increases the length of the liquid film in the evaporator, which becomes progressively thinner, with increasing wall heat flux (or power throughput). As the liquid film thickness in the evaporator, immediately above the liquid pool, reaches a critical value, δ_{cr} [7], it could break up into small rivulets separated by dry patches [4, 8] (Fig. 1b). The values of the power throughput and initial filling ratio of the working fluid for this type of liquid film dryout to occur, define the lower boundary of the CTPT operation envelope (Fig. 1b).

On the other hand, a high initial filling ratio of the working fluid, although avoiding liquid film dryout in the evaporator, could degrade the CTPT performance. Such performance degradation occurs as the liquid pool expands, due to boiling, with increasing wall heat flux, causing the length of the liquid film in the evaporator to become progressively shorter (Fig. 1c). Since the liquid film's heat transfer coefficient is significantly (more than an order of magnitude) higher than that of the pool [9, 10], as the liquid pool height increases (or the length of the liquid film in the evaporator decreases) the effective conductance of the CTPT evaporator decreases [11]. The values of the power throughput and initial filling ratio of the working fluid for when the expanding liquid pool fills the entire evaporator, define the upper boundary of the operation envelope (Fig. 1c). The closing boundary of the operation envelope corresponds to the power throughput at CCFL (Fig. 1d). This power throughput is independent of the filling ratio of the working fluid, but strongly depends on the type and vapor temperature of working fluid and CTPT dimensions [2–6].

In this paper, a one-dimensional, steady-state model is developed to determine the operation envelopes of CTPTs, as functions of the type, vapor temperature and initial filling ratio of the working fluid and the dimensions of thermosyphons. This model determines the upper and lower boundary of the operation envelope, according to the criteria mentioned earlier (Fig. 1b and c). The length of the liquid film and the liquid pool height in the evaporator section and the local thickness of the liquid film

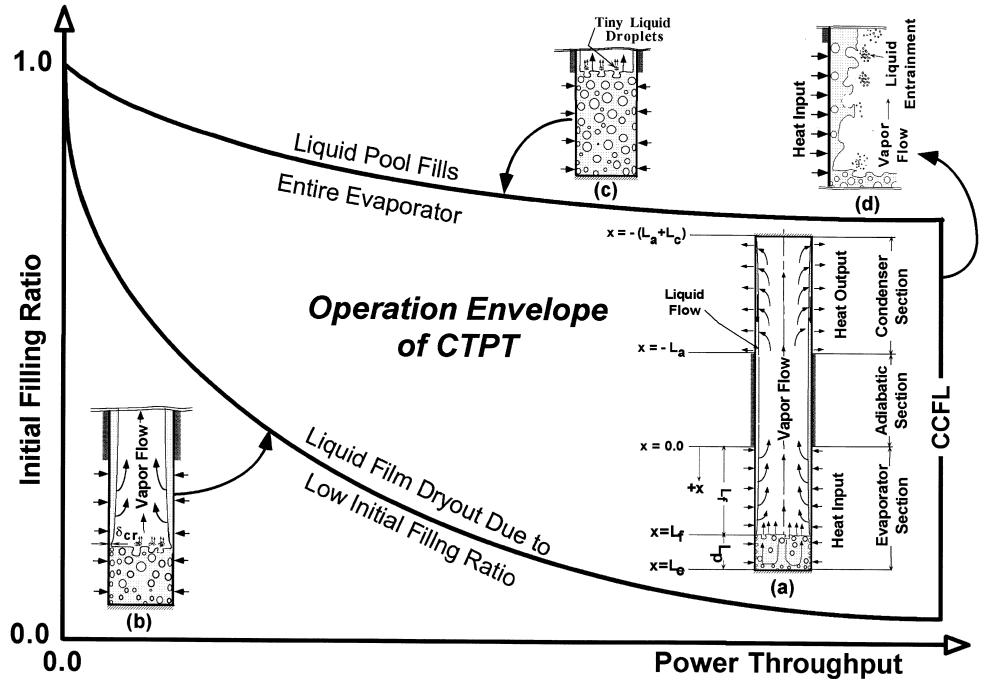

Fig. 1. A schematic of CTPT and illustrations of the conditions corresponding to the boundaries of the operation envelope.

along the thermosyphon wall, including the evaporator, adiabatic and condenser sections, are calculated as functions of the power throughput and the initial filling ratio of the working fluid.

In order to determine the expanding liquid pool height in the evaporator section, as a function of the type and initial filling ratio of the working fluid, CTPT dimensions and the power throughput, a semi-empirical correlation, based on experimental data of several working fluids [12], is developed. The corresponding length of the liquid film in the evaporator is then determined, since it is equal to the length of the evaporator section minus the calculated expanding liquid pool height. The calculated liquid pool height is compared with the evaporator section length to determine the conditions for the upper boundary of the operation envelope (Fig. 1c). To determine the conditions for the lower boundary of the operation envelope (Fig. 1b), the calculated liquid film thickness in the evaporator, immediately above the expanded liquid pool, is compared with the critical value, beyond which the film could dry out [4, 8].

The closing boundary of the CTPT operation envelope, corresponding to the CCFL at the exit of the evaporator (Fig. 1d), is determined using a separate model [5, 6]. The predictions of this model [5, 6] were within $\pm 10\%$ of the data of Prenger [13] and Reed and Tien [2] for methanol and the data of Nguyen-Chi and Groll [14] for water. The accuracy of the CCFL model [5, 6] stems from the fact that it expresses the interfacial shear stress as the sum of two components: (a) adiabatic shear stress, in the absence of evaporation at the interface and (b) dynamic shear stress, which accounts for the effect of evaporation at the L–V interface. More details on the CCFL model are available elsewhere [5, 6], and will not be repeated here due to space limitation.

A parametric analysis is also performed to investigate the effects on the CTPT operation envelope of the type and vapor temperature of the working fluid, the CTPT inner diameter and the lengths of the condenser, adiabatic and evaporator sections of the thermosyphon.

2. Model description

In this section, the model developed to calculate the upper and lower boundaries of the CTPT operation envelope is described. Also, the correlation developed to predict the expanding liquid pool height in the evaporator, as a function of the initial filling ratio, type and vapor temperature of working fluid, CTPT dimensions and the operation power throughput, is described and compared with experimental data of water, acetone and ethanol, at different initial filling ratios.

2.1. Lower boundary of CTPT operation envelope

The filling ratio of the working fluid in the evaporator section is determined from the overall mass balance in

the thermosyphon. This mass balance accounts for the liquid in the condenser and adiabatic sections and in the film and pool regions in the evaporator section and for the vapor in the thermosyphon cavity (Fig. 1a), as:

$$\xi = \frac{L_c}{L_e}[2\Delta_{mc} - \Delta_{mc}^2] + \frac{L_a}{L_e}[2\Delta_{ma} - \Delta_{ma}^2] + \frac{L_f}{L_e}[2\Delta_{mf} - \Delta_{mf}^2] + \frac{\rho_{mp}}{\rho_l}\left(1 - \frac{L_f}{L_e}\right) + \frac{\rho_g}{\rho_l}\left(\frac{L_c}{L_e}[1-\Delta_{mc}]^2 + \frac{L_a}{L_e}[1-\Delta_{ma}]^2 + \frac{L_f}{L_e}[1-\Delta_{mf}]^2\right). \quad (1)$$

The values of Δ_{mc} and Δ_{mf} are obtained from numerical integration of the calculated axial distribution of the liquid film thickness in the condenser and the evaporator sections, respectively (Fig. 1a). Since the liquid film thickness in the adiabatic section, Δ_{ma}, is constant and approximately equal to that at the exit of the evaporator, its value is determined from the mass balance of the working fluid at the exit of the evaporator. The liquid film thickness at the exit of the evaporator of a CTPT is typically 0.5–1.5 mm, depending upon the CTPT dimensions, the power throughput, and the type and vapor temperature of the working fluid [2, 5, 6]. Therefore, the effect of curvature can be neglected, and the liquid axial flow velocity, $u_l(x,y)$, calculated, with less than 5% error, from the solution of the momentum balance equation of the thin, falling liquid film, in Cartesian coordinates:

$$\mu_l \frac{\partial^2 u_l(x,y)}{\partial y^2} - \frac{dP(x)}{dx} = 0. \quad (2)$$

In equation (2), the axial pressure gradient in the liquid film can be expressed as [15]

$$\frac{dP(x)}{dx} = (4\tau_i(x)/d_g) + \Delta\rho g. \quad (3)$$

Combining equations (2) and (3) gives

$$\mu_l \frac{\partial^2 u_l(x,y)}{\partial y^2} - (4\tau_i(x)/d_g) - \Delta\rho g = 0. \quad (4)$$

This equation can be solved for $u_l(x,y)$, subject to the following boundary conditions:

$$u_l(x,0) = 0, \quad \tau_i(x) = -\mu_l \frac{\partial u_l(x,\delta)}{\partial y}. \quad (5)$$

These boundary conditions represent a non-slip condition at the wall-liquid interface and a non-zero interfacial shear at the liquid-vapor interface, τ_i, due to the counter-current vapor flow. This interfacial shear stress causes the maximum velocity of the liquid film in the evaporator to shift inward from the liquid–vapor interface toward the wall (Fig. 2). However, when the vapor flow is low (low power throughput) or the diameter of the thermosyphon is large, the vapor velocity, and hence the interfacial shear stress is negligibly small ($\tau_i \cong 0.0$). In this case, the maximum flow velocity occurs at the liquid film–vapor interface.

Equations (4) and (5) are expressed in dimensionless form as:

$$\frac{\partial^2 U(X,Y)}{\partial Y^2} - 8\tau_i^* + 2 = 0, \quad (6)$$

and

$$U(X,0) = 0, \quad \tau_i^* = -0.25\left(\frac{\Delta}{1-\Delta}\right)\frac{\partial U(X,1)}{\partial Y}. \quad (7)$$

Integrating equation (6), subject to the boundary conditions in equation (7), gives $U(X,Y)$, in terms of the dimensionless shear stress, $\tau_i^*(X)$, and the dimensionless liquid film thickness, $\Delta(X)$ as

$$U(X,Y) = -[1-4\tau_i^*]Y^2 + 2[1-2\tau_i^*((1+\Delta)/\Delta)]Y. \quad (8)$$

This equation can be rearranged to express the dimensionless interfacial shear stress in terms of the local Reynolds number, Re, and the two-phase Grashof number, Gr_{TP}, of the film as:

$$\tau_i^*(X) = (\Delta/(3+\Delta))[1-(6Re/\Delta^3 Gr_{TP}))]. \quad (9)$$

In equation (9), Re is obtained from the local mass balance of the working fluid in the different sections of the thermosyphon. Neglecting liquid entrainment in the vapor flow, which is true except when operating near the CCFL, and assuming thermal equilibrium at the liquid–vapor interface, the local film Reynolds number in the different sections of the thermosyphon can be expressed as:

(a) in condenser section

$$\{-(L_a/L_e + L_c/L_e) \leqslant X \leqslant -(L_a/L_e)\}$$

$$Re = (X(L_e/L_c) + (L_a/L_c) + 1)Re_{ext}, \quad (10a)$$

(b) in evaporator section

$$\{0 \leqslant X \leqslant (L_f/L_e)\}$$

$$Re = (1-X)Re_{ext}, \quad (10b)$$

(c) in adiabatic section

$$\{-L_a/L_e \leqslant X \leqslant 0\}$$

$$Re = Re_{ext}. \quad (10c)$$

2.2. Interfacial shear stress

As indicated earlier, the CCFL model used in the present analysis [6] expresses the shear stress at the liquid–vapor interface, $\tau_i^*(X)$, as the sum of two components: (a) the adiabatic shear stress, based on the adiabatic friction coefficient, f_{ia}, (i.e. in the absence of evaporation/condensation at the interface) [16, 17] and (b) the dynamic shear stress, recommended by Lee and Bankoff [18] and Linehan [19] to account for the effect of evaporation/condensation on the interfacial shear stress.

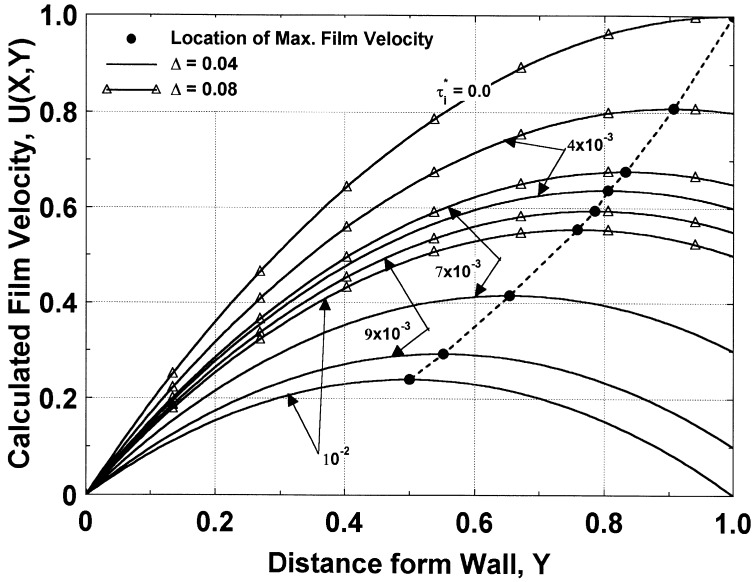

Fig. 2. Effect of interfacial shear on the lateral distribution of the liquid film velocity.

At high vapor flow, or high Re_{ext}, neglecting the dynamic shear stress, predicts CCFL to occur at a much lower Reynolds number, or a smaller liquid film thickness, at the exit of the evaporator, than in the experiments [2–6].

The interfacial shear stress in the CCFL model [6] is expressed as

$$\tau_i^*(X) = \tau_{ia}^*(X) \pm \tau_{id}^*(X). \quad (11)$$

The plus and minus signs of the second term on the right hand side of equation (11), account for the effect of condensation (in the condenser section) and evaporation (in the evaporator section) on the interfacial shear stress, respectively. As this equation indicates, evaporation reduces the interfacial shear stress while condensation increases the interfacial shear in the evaporator and the condenser section of the CTPT, respectively. The adiabatic and dynamics component of the interfacial shear stress in the CCFL model were expressed as [6, 18, 19]

$$\tau_{ia}^*(X) = f_{ia}(\Delta^4/(128(1-\Delta)))(\rho_g/\rho_l) \times Gr_{TP}(U_g(X)+U_i(X))^2, \quad (12a)$$

and

$$\tau_{id}^*(X) = (\Delta^2/(32(1-\Delta)))(d_i/L_e)Re_{ext}(U_g(X)+U_i(X)). \quad (12b)$$

In equation (12a), f_{ia}, is evaluated using one of the following correlations:

(a) Bharathan et al. [16]

$$f_{ia} = 0.005 + A\,Bo_\delta^b, \quad (13a)$$

where

$$\log_{10} A = -0.56 + 9.07 Bo^{-1}, \quad b = 1.63 + 4.74\,Bo^{-1}. \quad (13b)$$

(b) Grolmes et al. [17]

$$f_{ia} = 0.006 + A\,\delta^2(\mu_l/\mu_R)^{-.044}, \quad (14)$$

where $A = 2\times10^6$ m^{-2} and μ_R is a reference liquid viscosity = 1.0 CP.

The interfacial velocity of the falling film is obtained by substituting ($Y = 1.0$) into equation (8), yielding

$$U_i(X) = (24Re/Gr_{TP})A_1 + A_2 + A_3, \quad (15)$$

where

$$A_1 = [\Delta^3(\Delta+3)]^{-1}, \quad A_2 = (\Delta-1)/(\Delta+3),$$
$$A_3 = (\rho_g/\Delta\rho)(1-\Delta)/(\Delta+3). \quad (16)$$

The mean local vapor velocity, $U_g(X)$, is obtained from the local mass balance of the working fluid in the thermosyphon, which gives:

$$U_g(X) = (8Re_f/Gr_{TP})(\rho_l/\rho_g)[\Delta^2(1-\Delta)^2]^{-1}. \quad (17)$$

Substituting $U_i(X)$ and $U_g(X)$, from equations (15) and (17) into equation (11) gives $\tau_i^*(X)$ as

$$\tau_i^*(X) = [0.5f_{ia}(\rho_g/\rho_l)Gr_{TP}/(1-\Delta)] \times [(Re/Gr_{TP})A_4 + (\Delta^2/8)(A_2+A_3)]^2 \pm [Re_{ext}(d_i/L_e)/(1-\Delta)] \times [(Re/Gr_{TP})A_4 + (\Delta^2/8)(A_2+A_3)]. \quad (18)$$

Equating equations (9) and (18) gives the following transcendental equation for $\Delta(X)$

$$[0.5f_{ia}(\rho_g/\rho_l)Gr_{TP}/(1-\Delta)] \times [Re/Gr_{TP})A_4+(\Delta^2/8)(A_2+A_3)]^2 \pm [Re_{ext}(d_i/L_e)/(1-\Delta)] \times [(Re/Gr_{TP})A_4+(\Delta^2/8)(A_2+A_3)] = (\Delta/(\Delta+3))[1-(6Re/\Delta^3 Gr_{TP})]. \quad (19)$$

where

$$A_4 = (3/\Delta(\Delta+3))+((\rho_l/\rho_g)/(1-\Delta)^2). \quad (20)$$

Equation (19) is solved numerically for the axial distribution of the local liquid film thickness along the thermosyphon. The calculated liquid film thickness in the evaporator, immediately above the expanded boiling pool (Fig. 1b), is compared with the critical film thickness, Δ_{cr}, beyond which a film dryout could occur [7]:

$$\Delta_{cr} = 2d_i^{-1}[18v_l q_e(-d\sigma/dT)/(Cp_l(\rho_l g)^2)]^{0.25}, \text{or}$$
$$\Delta_{cr} = 18(\Delta\rho/\rho_l)(Re_{ext}/Gr_{TP})((h_{fg}/(\rho_l Cp_l g)) \times (-d\sigma/dT)/(d_i L_e)). \quad (21)$$

In order to solve equation (19), however, the expanded liquid pool height has to be determined. This is accomplished using the semi-empirical correlation developed in the next section and verified by comparing its predictions with experimental data for a number of working fluids [12].

2.3. Expanding liquid pool height correlation

The height of the expanding liquid pool in the CTPT evaporator can simply be expressed as:

$$H_p = 4m_{lp}/(\pi L_e d_i^2 \rho_{mp}). \quad (22)$$

where m_{lp} is determined from equation (1) while the mean density of the liquid pool is given in terms of its mean void fraction, α_m, as:

$$\rho_{mp} = \alpha_m \rho_g + (1-\alpha_m)\rho_l. \quad (23)$$

The pool mean void fraction in equation (23) is calculated as follows:

$$\alpha_m = (1-(L_f/L_e))^{-1}\int_{(L_f/L_e)}^{1} \alpha(X)\,dX. \quad (24)$$

The local void fraction in the pool, $\alpha(X)$, is obtained from the drift flux model [20] after substituting zero for the liquid flux in the pool, as

$$\alpha(X) = J_g(X)[C_o J_g(X)+\langle V_{gj}\rangle]^{-1}, \quad (25a)$$

where

$$\langle V_{gi}\rangle = V_{gj}^{+}(\sigma g(\rho_l-\rho_g)/\rho_l^2)^{0.25}. \quad (25b)$$

The distribution coefficient, C_o, for round tubes, typically used for CTPT, is given as [20]:

$$C_o = 1.2\text{–}0.2\sqrt{\rho_g/\rho_l}. \quad (26)$$

The vapor local mass flux in equation (25) is given from the energy balance in the pool

$$J_g(x) = (4q_e L_e/(\rho_g d_i h_{fg}))(1-X). \quad (27)$$

The dimensionless vapor drift velocity in equation (25b), V_{gj}^{+}, is given, in terms of the liquid viscosity number, $N_{\mu f}$, and the pool's hydraulic diameter, D_h, as [20].

(a) at low viscosity number, $N_{\mu f} < 2.5\times10^{-3}$:

$$V_{gj}^{+} = 0.0019 D_h^{0.809}(\rho_l/\rho_g)^{0.157}N_{\mu f}^{-0.562}, \quad \text{for } D_h \leqslant 30 \quad (28a)$$

$$V_{gj}^{+} = 0.03(\rho_l/\rho_g)^{0.157}N_{\mu f}^{-0.562}, \quad \text{for } D_h > 30 \quad (28b)$$

(b) at high viscosity number, $N_{\mu f} > 2.5\times10^{-3}$

$$V_{gj}^{+} = 0.92(\rho_l/\rho_g)^{0.157}, \quad \text{for } D_h \geqslant 30 \quad (28c)$$

The calculated liquid pool height using equation (22), in conjunction with equations (23)–(28), is compared with the experimental data for acetone (Fig. 3a), ethanol (Fig. 3b) and water (Fig. 3c) at different initial filling ratios [12]. In both the data and the calculations, the physical properties of the working fluids are evaluated at the average pool temperature. These figures indicate the excellent agreement of equation (22) with the experimental data of all three working fluids, to within $\pm 8\%$ (Fig. 4). Fig. 3a–c also show that the expanding liquid pool height increases with increasing either the vapor velocity (or input power to the evaporator), or the initial filling ratio of the working fluid.

3. Results and discussion

Figure 5 presents the calculated operation envelope for an ammonia CTPT. The upper and lower boundaries of the envelope are in excellent agreement with the experimental observations and data of Unk and Bartsch [1]. The predictions of the lower boundary by Unk and Bartsch [1], however, were significantly higher than their own experimental data.

The upper and lower boundaries of the CTPT operation envelope intersect at a zero power throughput and an initial filling ratio of unity, $\xi = 1.0$ (Figs 1 and 5). For both the upper and lower boundaries of the operation envelope, the initial liquid inventory in the pool decreases with increasing power throughput. The values of the initial filling ratio corresponding to these two boundaries also diverge as the power throughput increases. Eventually, the CCFL is reached as liquid entrainment occurs at the exit of the evaporator [2–6].

In Fig. 5, the CCFL for the ammonia thermosyphon at $T_v = 288$ K, occurred at a power throughput of 1550 W (or $Re_{ext} = 450$). Slightly below this value, the operation envelope extends from an initial filling ratio of 0.219–0.515. A filling ratio below 0.219 would cause the liquid film in the evaporator to break up into a series of liquid

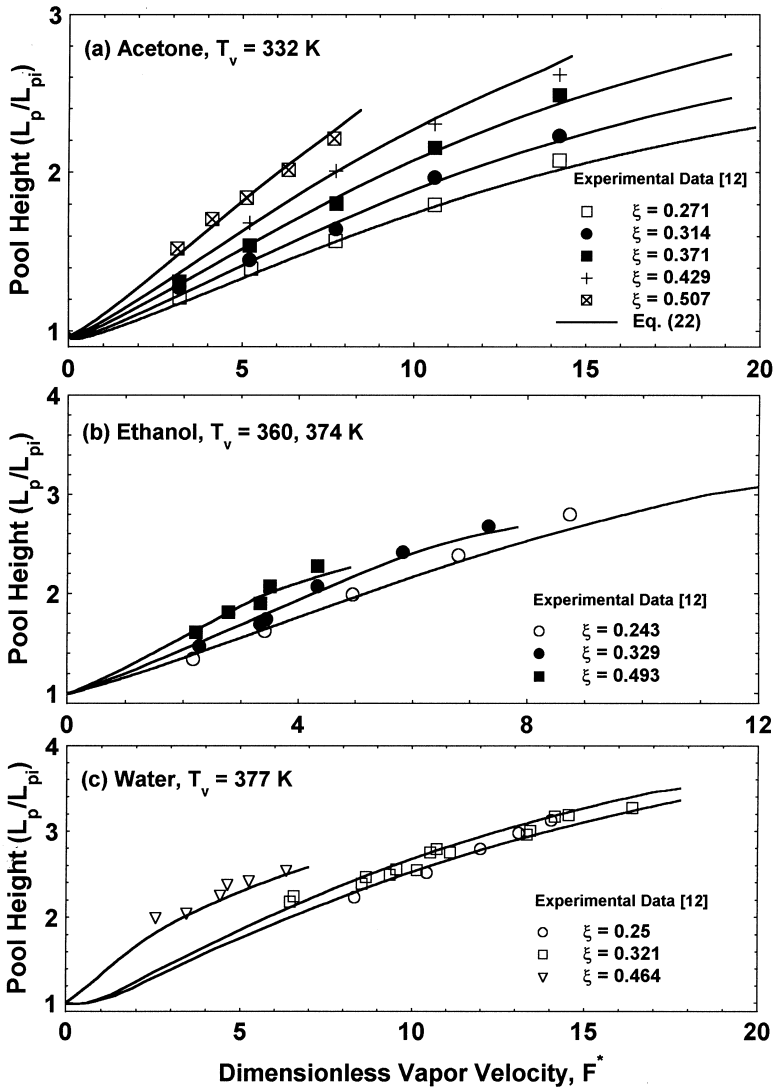

Fig. 3. Effect of dimensionless vapor velocity on the expanding liquid pool height for different working fluid.

rivulets, separated by dry patches [4, 8]. On the other hand, for initial filling ratios higher than 0.515, the boiling liquid pool would expand, filling the entire volume of the evaporator, hence, degrading the performance of the thermosyphon.

3.1. Effect of CTPT adiabatic and condenser section length

Figure 6a and b shows the effects on the CTPT operation envelope of the lengths of the adiabatic and the condenser sections, respectively. Increasing either length increases the initial filling ratios corresponding to the upper and lower boundaries of the operation envelope, but insignificantly changes the operation envelope's area. Changing the length of either the adiabatic or the condenser section does not affect the value of power throughput at the CCFL.

3.2. Effect of CTPT inner diameter

Increasing the inner diameter of the thermosyphon increases the initial filling ratios for the upper and lower boundaries of the operation envelope (Fig. 7a and b) At the same power throughput, the increase in the filling ratio for the former, however, is larger than that for the later, resulting in a net increase in the envelope's operation area. Figure 7a and b shows that for a given CTPT

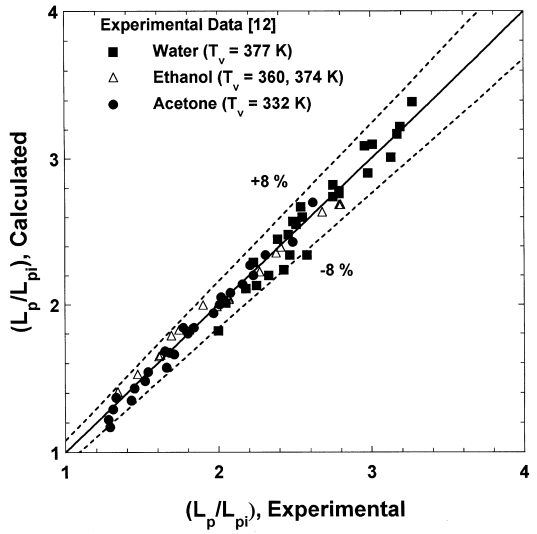

Fig. 4. Comparison of experimental and calculated expanded pool heights.

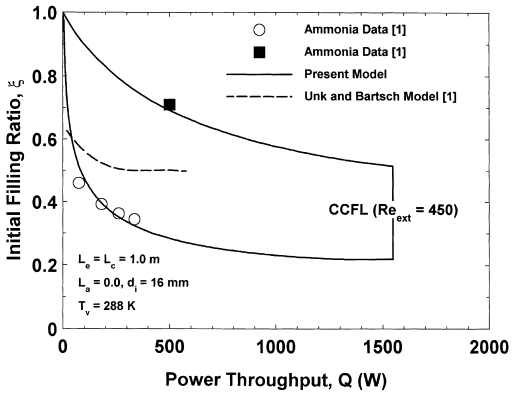

Fig. 5. Comparison of the model prediction of the operation envelope for an ammonia CTPT with experimental data [1].

inner diameter, increasing the power throughput decreases the values of the initial filling ratio corresponding to the envelope's upper and lower boundaries. Increasing the inner diameter of the thermosyphon significantly increases the area of the operation envelope, because it raises the upper boundary more than the lower boundary of the envelope and significantly increases the power throughput corresponding to the CCFL. Such an increase in the CCFL power throughput is because increasing the inner diameter of the thermosyphon decreases the vapor velocity, lowering the interfacial shear stress at the liquid–vapor interface, τ_i^*. Consequently, as the inner diameter of the thermosyphon increases, CCFL occurs at a much higher power throughput (or higher Re_{ext}).

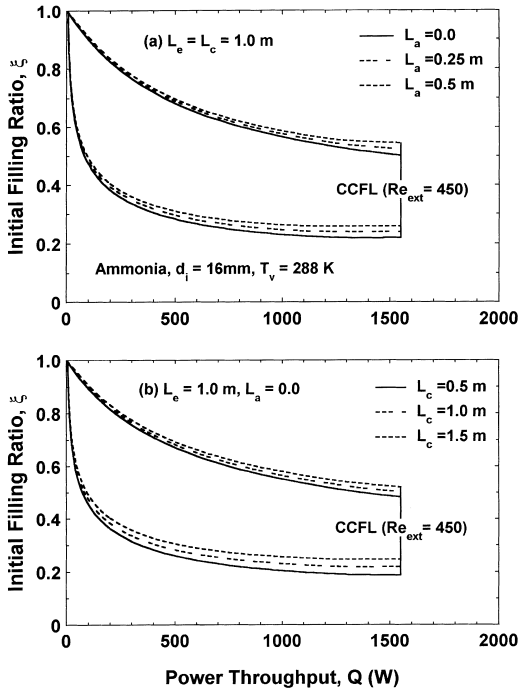

Fig. 6. Effect of adiabatic and condenser lengths on the operation envelope of CTPT.

Figure 7c indicates that the lower boundary of the operation envelope for the acetone CTPT falls below that for methanol, but is higher than that for ethanol, for all values of the inner diameter shown. When $d_i \leqslant 28.55$ mm, the upper boundary for methanol falls below that for ethanol, but is higher than that for acetone. For the intermediate values of the CTPT inner diameter (28.55 mm $< d_i \leqslant 37.28$ mm), the operation envelope's upper boundary for ethanol falls below that for methanol, but is higher than that for acetone. For large CTPT inner diameters, $d_i \geqslant 37.28$ mm, however, the operation envelope's upper boundary for acetone is below that for methanol, but higher than that for ethanol. The operation envelope's upper boundary for ammonia is significantly higher than those of the other four working fluids (methanol, ethanol, water and acetone).

3.3. Effect of CTPT evaporator length

Figure 8a indicates that decreasing the length of the evaporator section generally decreases the useful area of the operation envelope, but increases the power throughput corresponding to CCFL. Increasing the evaporator length lowers the upper boundary and, to a larger extent, the lower boundary of the operation envelope. At the same vapor temperature and evaporator wall heat flux, the critical liquid film thickness corresponding to the

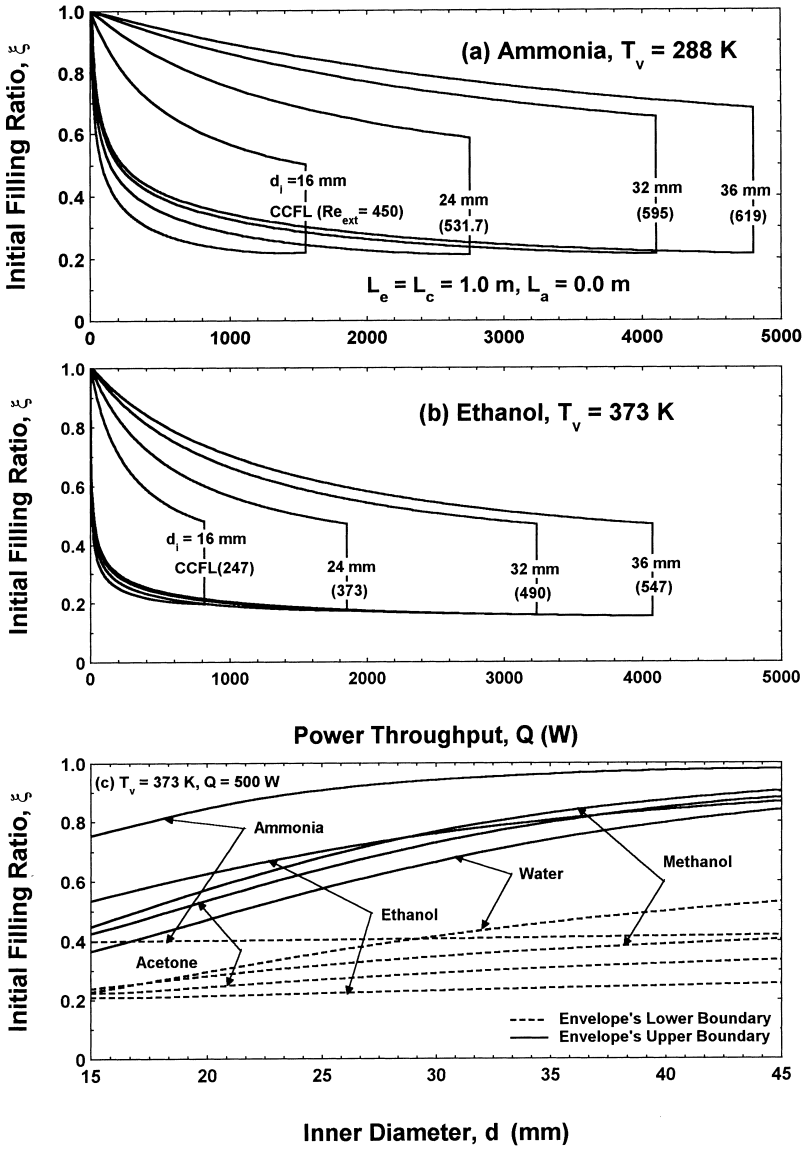

Fig. 7. Effect of inner diameter on the operation envelope of different CTPT working fluids.

lower boundary of the operation envelope (Fig. 1b) is independent on the evaporator length, equation (21). For the same power throughput, however, decreasing the evaporator length increases the evaporator wall heat flux and, hence, the critical liquid film thickness. Such an increase in the critical liquid film thickness causes the liquid film length to decrease (or the liquid pool height to increase). Therefore, for the same power throughput, decreasing the evaporator length raises the initial working fluid filling ratio corresponding to the lower boundary of the CTPT operation envelope (Fig. 8a).

Figure 8b shows that the initial filling ratio corresponding to the envelope's upper boundary decreases, as the pool mean void fraction increases with increasing the wall heat flux in the evaporator. Also, for the same evaporator heat flux, increasing the evaporator length decreases the initial filling ratio, but increases the pool mean void fraction, corresponding to the upper boundary of the operation envelope. The effect of changing the evaporator length on the upper and lower boundaries of the CTPT operation envelope depends not only on the vapor temperature and inner diameter of the thermosyphon, but also on the type of the working fluid (Fig. 8c).

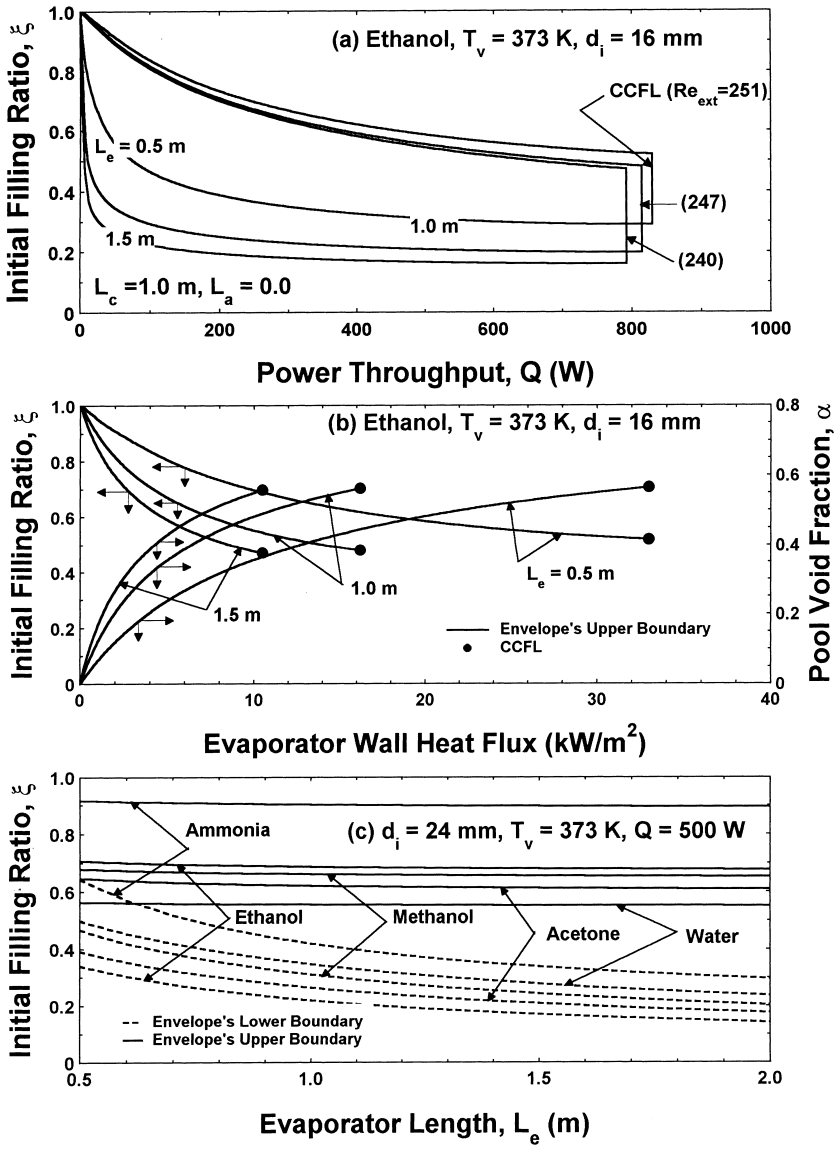

Fig. 8. Effect of power throughput, evaporator wall heat flux, and evaporator length on the operation envelope of different CTPT working fluids.

Figure 8c shows that the values of the initial filling ratio for the upper boundary of the operation envelope are almost independent of the evaporator length. Increasing the evaporator length, however, significantly decreases the initial filling ratios for the lower boundary of the operation envelope. For a given evaporator length, the initial filling ratios for the upper boundary of the methanol envelope are below those for ammonia and ethanol, but higher than those for acetone and water (Fig. 8c). Also, the initial filling ratios for the lower boundary for methanol CTPT are below those for ammonia and water, but higher than those for acetone and ethanol.

3.4. Critical liquid film thickness in CTPT evaporator

The results presented in Fig. 8 show the effect of changing the vapor temperature and the type of working fluid on the critical liquid film thickness in the evaporator (Fig. 1b). The critical liquid film thickness increases with increasing the power throughput, or decreasing the vapor temperature (Fig. 9a). Both parameters result in a higher

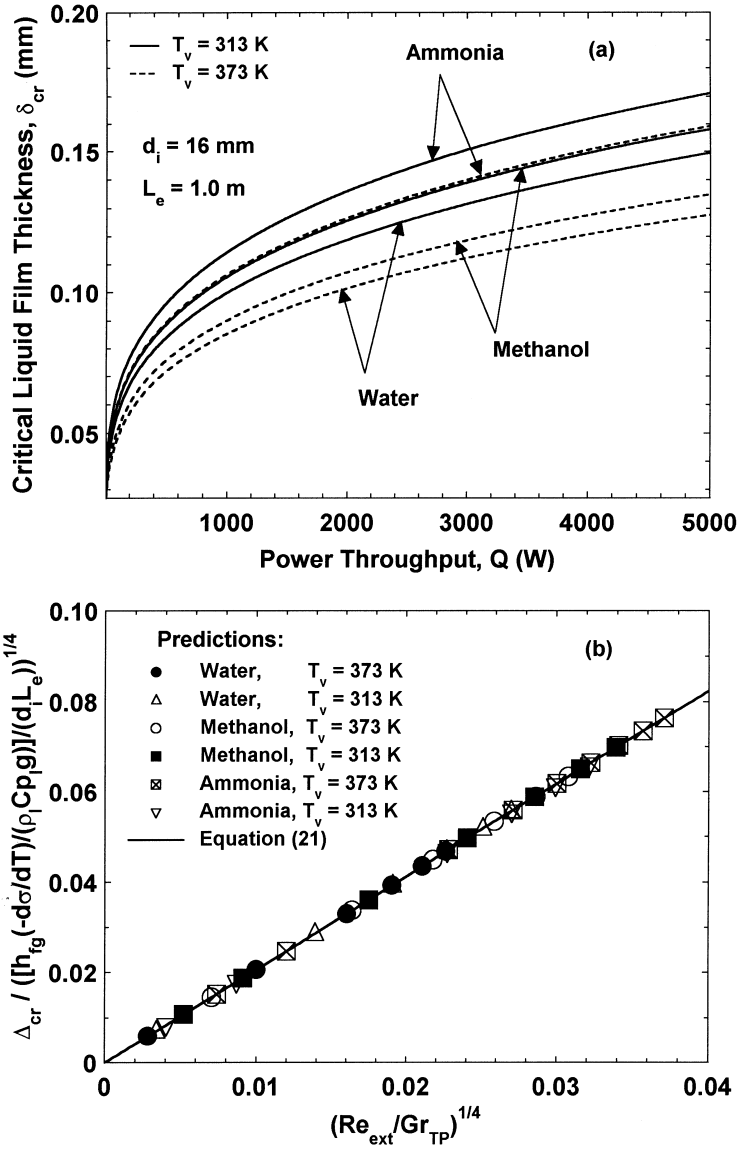

Fig. 9. Effects of power throughput and of $(Re/GR_{TP})^{1/4}$ on the critical liquid film thickness in the evaporator section.

evaporation rate from the liquid film, thus requiring that, unless the liquid film thickness increases due to liquid flow from the condenser, it would dry out. As delineated in Fig. 9a, at power throughput of 2000 W and vapor temperature of 313 K, the critical film thickness for ammonia, methanol and water is 0.136, 0.126 and 0.119 mm, respectively. At this temperature, the vapor pressures of these working fluids are 1534, 40 and 7 kPa, respectively. For generalization of the results, Fig. 9b plots the dimensionless critical liquid film thickness in the evaporator versus $(Re_{ext}/Gr_{TP})^{0.25}$. The results for all working fluids fall on a straight line represented by equation (21), regardless of the vapor temperature of the working fluid and the CTPT dimensions.

3.5. Effect of type of working fluid

Figures 10a and b compares the operation envelops of acetone, ethanol and methanol CTPTs at vapor temperatures of 373 and 333 K, respectively. Increasing the vapor temperature increases significantly the area of the operation envelope, by shifting the right boundary corresponding to the CCFL to a higher power throughput. The power throughput at CCFL increases with increasing

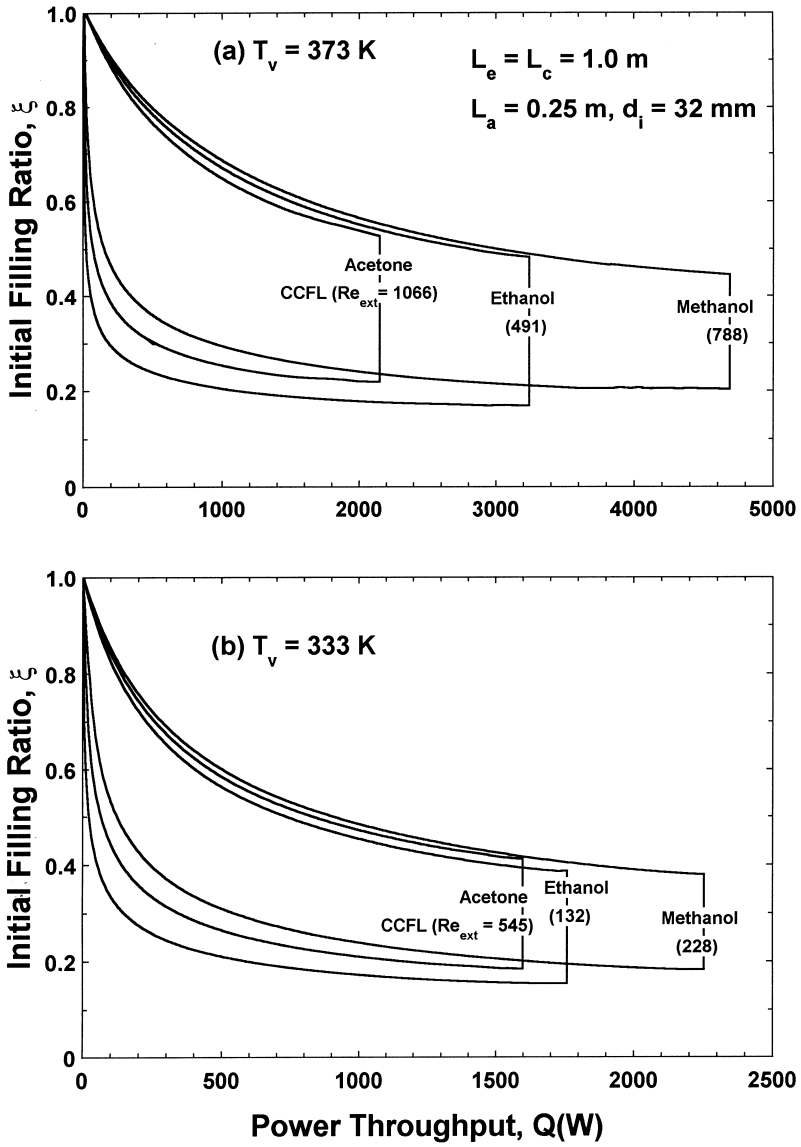

Fig. 10. Effect of the type of working fluid and vapor temperature on the operation envelope of different CTPT working fluids.

the latent heat of vaporization of the working fluid [5, 6]. For example, at 373 K, the latent heat of vaporization for methanol, ethanol and acetone are 1011.5, 810.0 and 470.0 kJ kg^{-1}, respectively, and their corresponding power throughputs at CCFL are 4685.8, 3243.0 and 2149.4 W, respectively. As shown in Fig. 10b, these values decrease as the vapor temperature decreases. At a vapor temperature of 333 K, the power throughput at CCFL for methanol, ethanol and acetone decreases to 2252.9, 1760.3 and 1599.5 W, respectively. For a given wall heat flux, the high latent heat of vaporization lowers the vapor flow rate at the exit of the evaporator, resulting in a lower interfacial shear stress, increasing the power throughput at the CCFL [5, 6].

3.6. Effect of CTPT vapor temperature

Figure 11 shows that increasing the vapor temperature of the working fluid also increases the initial filling ratios corresponding to the upper and lower boundaries of the CTPT operation envelope. Increasing the vapor temperature decreases the mean void fraction in the liquid pool, thus increasing the initial working fluid filling ratios for the upper boundary of the operation envelope. Con-

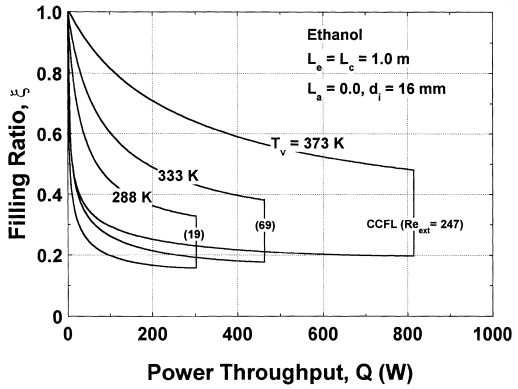

Fig. 11. Effect of vapor temperature on the operation envelope of an ethanol CTPT.

versely, increasing the vapor temperature decreases the critical liquid film thickness (Fig. 9a), but increases the length of the liquid film in the evaporator, raising the initial filling ratios for the lower boundary of the operation envelope.

Increasing the vapor temperature also increases the power throughput for the closing boundary of the operation envelope, corresponding to the CCFL. Such an increase in CCFL is due to the decrease in the liquid viscosity, which lowers the interfacial shear stress at the exit of the evaporator [5, 6]. In summary, increasing the vapor temperature of the working fluid, increases significantly the useful area of the CTPT operation envelope, by raising the upper boundary and, to a lesser extent, the lower boundary and shifting the CCFL boundary to higher power throughput (or higher Re_{ext}).

3.7. Performance isotherms

For a given wall superheat in the evaporator (temperature difference between the inner wall of the evaporator and the vapor in thermosyphon), the performance of a CTPT can be quantified in terms of the achievable operation power throughput, as:

$$Q = U_{ei}A_{ei}(\bar{T}_{ei} - T_v) = U_{ei}A_{ei}\Delta T_e, \tag{29}$$

where the overall conductance of the CTPT evaporator is given as:

$$U_{ei} = \left(\frac{(L_p/L_e)}{h_p} + \frac{(L_f/L_e)}{h_f}\right)^{-1}. \tag{30}$$

In equation (30), the expanded liquid pool height in the evaporator, L_p, is given by equation (22) and the liquid film length, $L_f = (L_e - L_p)$.

The heat transfer coefficients in the liquid film and pool regions in the evaporator depend on the prevailing heat transfer regime in each region. Recently, El-Genk and Saber [9, 10] developed heat transfer correlations for the liquid film and pool regions which provided smooth transition between the various heat transfer regimes in each region and agreed with experimental data for each regime to within $\pm 15\%$. The heat transfer coefficient in the liquid pool regime is given as [10]:

$$h_p = (h_{NC}^4 + h_{PNB}^4)^{0.25}, \tag{31}$$

where

$$h_{NC} = 0.475(k_l/d_i)Ra^{0.35}(l_m/d_i)^{0.58}, \tag{32}$$

$$h_{PNB} = (1.0 + 4.95\psi)h_{Ku}, \tag{33}$$

$$h_{Ku} = 6.95x10^{-4}(k_l/l_m)Pr_l^{0.35}(q_e l_m/(\rho_g h_{fg} v_l))^{0.7}(Pl_m/\sigma)^{0.7}, \tag{34}$$

$$\Psi = (\rho_g/\rho_l)^{0.4}\{(Pv_l/\sigma)[\rho_l^2/(\sigma g(\rho_l - \rho_g))]^{0.25}\}^{0.25}. \tag{35}$$

Similarly, the liquid film heat transfer coefficient in the evaporator is given as [9]:

$$h_f = (h_x^3 + h_{FNB}^3)^{1/3}, \tag{36}$$

where

$$h_x = (4/3)^{1/3}(k_l/l_l)Re^{-1/3}, \quad \text{and} \tag{37}$$

$$h_{FNB} = 1.155x10^{-3}(k_l/l_l)N_{\mu f}^{0.33}Pr_l^{0.35} \times (q_e l_m/(\rho_g h_{fg} v_l))^{0.7}(Pl_m/\sigma)^{0.7}. \tag{38}$$

Figure 12 presents the calculated performance isotherms of an ethanol CTPT. It shows that the useful operation ranges of the power throughput and initial filling ratio strongly depend on the wall superheat in the evaporator, ΔT_e. These ranges increase with increasing wall superheat, until the CTPT performance isotherms intersect the CCFL boundary, where $2.0\ \text{K} < \Delta T_e < 2.5\ \text{K}$. Beyond this point, increasing the wall superheat decreases the useful operation ranges of both the power throughput and the initial filling ratio of working fluid.

Based on the results in Fig. 12, the widest operation

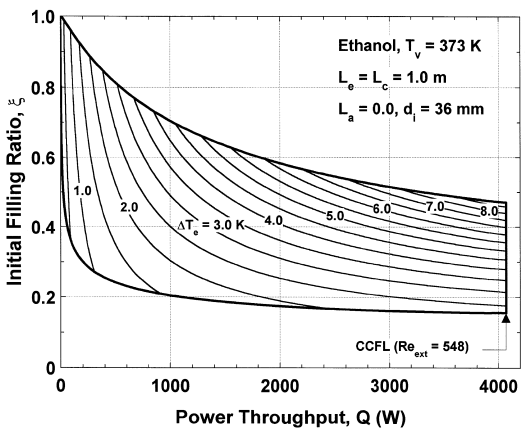

Fig. 12. Calculated performance isotherms within the operation envelope of an ethanol CTPT.

ranges of the power throughput and the initial filling ratio for the ethanol CTPT occur at a wall superheat of ~ 2.25 K. This wall superheat changes, however, with the vapor temperature, the inner diameter of thermosyphon and the type of working fluid. The effects of these parameters on the performance isotherms within the operation envelopes of CTPTs are not investigated in this paper because of limitation on the total length of the text.

In practical applications, however, calculating the performance isotherms, such as those shown in Fig. 12 for ethanol, would help the CTPT designer select the proper values of the initial filling ratio of the working fluid, for particular ranges of power throughput and wall superheat in the evaporator. For example, at a power throughput of 2500 W, in order for the ethanol CTPT in Fig. 12, to operate with its envelope, $2.0 < \Delta T_e < 7.0$ K. For this range of the wall superheat, the initial filling ratio of ethanol varies from 0.166 to as much as 0.545, respectively.

4. Summary and conclusions

A one-dimensional steady-state model is developed to predict the operation envelope and performance isotherms of CTPTs. The model calculates the length of the liquid film and expanding liquid pool in the evaporator, as functions of the power throughput, type and vapor temperature of the working fluid, and CTPT dimensions. The model also calculates the local thickness of the liquid film along the thermosyphon, including the evaporator wall.

The values of the initial filling ratio of the working fluid and the power throughput for when the liquid film thickness in the evaporator, immediately above the pool region, equals a critical thickness [7], define the lower boundary of the CTPT operation envelope (Fig. 1b). Also, the initial filling ratios of the working fluid and the power throughputs for when the expanding liquid pool height fills the entire evaporator section, define the upper boundary of the CTPT operation envelope (Fig. 1c). In order to determine the expanding liquid pool height in the evaporator section, a semi-empirical correlation is developed, based on the drift flux model [20]. The predictions of the developed correlation agree with the experimental data of water, ethanol and acetone [12], to within $\pm 8\%$. The model predictions of the operation envelope's upper and lower boundaries are also in excellent agreement with the experimental observations and the data for an ammonia CTPT [1]. The third and closing boundary of the CTPT operation envelope (Fig. 1d), corresponding to the power throughput at CCFL, is determined using a separate model [5, 6].

A parametric analysis is performed to investigate the effects of the type of working fluid, vapor temperature, CTPT inner diameter and the lengths of the condenser, adiabatic and evaporator sections on the operation envelope. The most important effects are these of the CTPT inner diameter, evaporator length and vapor temperature. Increasing the inner diameter significantly expands the operation envelope, by increasing the power throughput corresponding to CCFL and raising the upper boundary and, to a lesser extent, the lower boundary of the envelope. For the same thermosyphon inner diameter, increasing the length of the condenser or the adiabatic section slightly changes the area of the CTPT operation envelope. The lengths of these sections, however, do not change the value of the power throughput corresponding to CCFL, but raise the envelope's upper and lower boundaries by almost the same amount.

Results also show that increasing the vapor temperature and/or the evaporator length significantly increases the area of the CTPT operation envelope. Higher vapor temperature raises the envelop's upper boundary and, to a lesser extent, the lower boundary and shifts the CCFL boundary to a higher power throughput. The calculations demonstrated that the present model of the CTPT operation envelope could be used as an effective design tool. The demonstrated ability of this model would help selecting the proper CTPT dimensions and the type, vapor temperature, and the initial filling ratio of the working fluid for meeting the power throughput requirements of a given industrial application, without risking a dryout of the liquid film in the evaporator section.

Acknowledgement

Research sponsored by the University of New Mexico's Institute for Space and Nuclear Power Studies.

References

[1] J. Unk, G. Bartsch, A contribution to the theory of the closed two-phase thermosyphon, advances in phase change heat transfer, in: X. Mingdao (Ed.), Proceedings of International Symposium on Phase Change Heat Transfer, Chongqing, Sichuan, China, Institute of Engineering Thermophysics, Chongqing University. 1988, pp. 563–566.

[2] J.G. Reed, C.L. Tien, Modeling of the two-phase closed thermosyphon, J. Heat Transfer, 109 (1987) 722–730.

[3] Z.J. Zuo, F.S. Gunnerson, Numerical study of the thermosyphon flooding limit, Fund. of Heat Pipes, ASME HTD-Vol. 278 (1994).

[4] S. Roesler, M. Groll, Flow visualization and analytical modeling of interaction phenomena in closed two-phase flow systems, Proceedings of the Eighth International Heat Pipe Conference, Beijing, China, Institute of Engineering Thermophysics, Chinese Academy of Sciences, 1992, pp. 26–32.

[5] M.S. El-Genk, H. Saber, Effect of dynamic shear stress on thermosyphon flooding limit, AIChE Symposium Series, 92 (1996) 342–348.
[6] M.S. El-Genk, H. Saber, Flooding limit in closed, two-phase flow thermosyphons, Int. J. Heat and Mass Transfer 40 (9) (1997) 2147–2164.
[7] T. Fujita, T. Ueda, Heat transfer to falling liquid films and film breakdown—I, Subcooled liquid film, Int. J. Heat and Mass Transfer 21 (1978) 97–108.
[8] F.E. Andros, Heat transfer characteristics of the two-phase closed thermosyphon (wickless heat pipe) including direct flow observation, Ph.D. Dissertation, Arizona State University, Tempe, AZ, 1980.
[9] M.S. El-Genk, H. Saber, Heat transfer correlations for liquid film in the evaporator of enclosed, gravity-assisted thermosyphons, J. Heat Transfer 102 (1998) 477–484.
[10] M.S. El-Genk, H. Saber, Heat transfer correlations for small, uniformly heated liquid pools, Int. J. Heat and Mass Transfer 41(2) (1998) 261–274.
[11] M.S. El-Genk, H. Saber, Thermal conductance of the evaporator section of closed two-phase thermosyphons (CTPTs), Proceedings of the Seventh AIAA/ASME Joint Thermophysics and Heat Transfer Conference, Albuquerque, NM, 15–18 June, 1998, pp. 99–106.
[12] H. Jialun, Ma. Tongze, Z. Zhengfang, Investigation of boiling liquid pool height of a two-phase closed thermosyphon, in: M. Tongze (Ed.), Proceedings of the Eighth International Heat Pipe Conference, Beijing, China, Inst. of Eng. Thermophysics, Chinese Academy of Sciences, 1992, pp. 154–159.
[13] F.C. Prenger, Performance limits of gravity-assisted heat pipes, Proceedings of the Fifth International Heat Pipe Conference, Part 1, 1984, pp. 1–5.
[14] H. Nguyen-Chi, M. Groll, Entrainment for flooding limit in a closed two-phase thermosyphon, in: D.A. Reay (Ed.), Advances in Heat Pipe Technology, Pergamon Press, New York, 1981, pp. 147–162.
[15] J.C.B. Lopse, A.E. Dukler, Droplet entrainment in vertical annular flow and its contribution to momentum transfer, AICHE J. 32 (9) (1986) 1500–1515.
[16] D. Bharathan, G.B. Wallis, H.J. Richter, Air–water countercurrent annular flow, EPRI Report No. EPRI NP-1165, 1979.
[17] M.A. Grolmes, G.A. Lambert, H.K. Fauske, Flooding in vertical tubes, AIChE Symposium Series No. 38, Multiphase Flow Systems, Paper No. A4, 1974.
[18] S.C. Lee, S.G. Bankoff, Stability of steam–water countercurrent flow in an inclined channel: flooding, J. Heat Transfer 105 (1983) 713–718.
[19] J.H. Linehan, The interaction of two-dimensional stratified, turbulent air–water and steam–water flows, Ph.D. dissertation, University of Wisconsin, 1968.
[20] I. Kataoka, M. Ishii, Drift flux model for large diameter pipe and new correlation for pool void fraction, Int. J. Heat and Mass Transfer 30 (9) (1987) 1927–1939.